

Variability of accretion flow in the core of the Seyfert galaxy NGC 4151

B. Czerny¹, V.T. Doroshenko², M. Niño-Lacort¹, A. Schwarzenberg-Czerny^{1,3},
Z. Loska¹ and G. Madejski⁴

¹*N. Copernicus Astronomical Center, Bartycka 18, 00-716 Warsaw, Poland*

²*Crimean Laboratory of Sternberg Astronomical Institute, Nauchny, Crimea, 98409 Ukraine*

³*Astronomical Observatory of Adam Mickiewicz University, ul. Słoneczna 36, 60-286 Poznań, Poland*

⁴*Stanford Linear Accelerator Center, Menlo Park, CA 91025, USA*

2 December 2024

ABSTRACT

We analyze observations of the galaxy NGC 4151 covering 90 years in the optical band and 27 years of the 2–10 keV X-ray band. We compute the Normalized Power Spectrum Density (NPSD), the Structure Function (SF) and the Autocorrelation Function (ACF) for these data. The results show that the optical and X-ray variability are essentially different. X-ray variations are predominantly in the timescale range of 10 – 1000 days. The optical variations have also a short timescale component which is related to X-ray variability but the dominant effect is the long timescale variability, with timescales of order of ~ 12 years. We compare our results with observations of NGC 5548 and Cyg X-1. We conclude that the long timescale variability may be caused by radiation pressure instability in the accretion disk, although the observed timescale in NGC 4151 is by a factor of few longer than expected. X-ray variability of this source is very similar to what is observed in Cyg X-1, if scaled down with the mass of the black hole, which suggests that the radiation pressure instability does not affect considerably the X-ray production.

Key words: galaxies: active – galaxies:individual:NGC4151 – instabilities – X-rays:galaxies.

1 INTRODUCTION

NGC 4151 ($z=0.00332$; $D=13.2$ Mpc assuming Hubble constant $75 \text{ km s}^{-1} \text{ Mpc}^{-1}$) is one of the classical Seyfert 1 galaxies. It is probably the most frequently observed AGN and therefore a perfect object for studies although it is both typical, and atypical, for its class, as nicely and extensively summarized by Ulrich (2000). We therefore chose it as a second source (after NGC 5548; Czerny, Schwarzenberg-Czerny & Loska 1999) for which the nature of the variability can be studied by computing the power spectrum density (hereafter PSD) in the *optical band and X-ray band*.

The host galaxy is a typical spiral galaxy SAB(rs)ab of 11.3 mag brightness in B band (Perez et al. 1998). The extinction due to the Galaxy is low ($A_V < 0.01$ in B band) because NGC 4151 is located nearby the North Galaxy Pole ($b_{\text{II}} = 75.1^\circ$). But there is an intrinsic extinction in NGC 4151 and in the optical region the extinction is equal $A_V = 1^m.0$ in BLR and $A_V = 0^m.7$ in NLR (Ward et al. 1987). Direct estimates in the UV bands give much less extinction ($E_{B-V} = 0.06$) for wavelength $\lambda 2200 \text{ \AA}$ and fits to $A_V = 0^m.18$ (Wu & Weedman 1978). The hydrogen col-

umn density inferred from the equivalent widths of ultraviolet absorption CIII lines is about $1.7 \times 10^{19} \text{ cm}^{-2}$ (Kriss et al. 1992) and it's smaller in comparison with X-ray column density. The X-ray observations clearly indicate that the nucleus itself is significantly obscured for X-ray continuum ($N_H = (1 - 10) \times 10^{22} \text{ cm}^{-2}$) (Yaqoob et al. 1993). It corresponds to $A_V \approx 5^m - 50^m$ according to the standard relation between A_V and N_H from Reina & Tarengi (1973).

HST observations suggested that the line of sight towards the nucleus (at least in the epoch when the observation was performed - on 1991 June 18/19) lies outside the ionization cone (Evans et al. 1993). However, broad emission lines are usually well visible although with superimposed absorption features (e.g. Brandt et al. 2001); only in 1984 the broad component of H_β was absent (Lyutyj, Oknyanskij & Chuvpov 1984; Penston & Pérez 1984; see also Pronik, Sergeev & Sergeeva 2001) and the spectrum more closely resembled that of a narrow emission line or a Seyfert 2 type galaxy. Therefore it seems the most of time, the nucleus is viewed directly and the scattered component characteristic for Seyfert 2 galaxies does not dominate the spectrum, apart from the soft X-ray band (see Ogle et al. 2000).

Regardless of the fact that X-ray extinction is high, the intrinsic X-ray spectrum seems to be fairly typical for a Seyfert galaxy (Zdziarski, Johnson & Magdziarz 1996).

The brightness of the nucleus varies dramatically in all timescales and energy bands. Spectrum and variability in the 50–150 keV band was studied by Johnson et al. (1997) (almost a factor of 2 variability in days and years). 2–10 keV variability was studied in more detail using Fourier analysis. It was found (Papadakis & McHardy 1995) that X-ray power spectrum of NGC 4151 covering the range $10^{-6} - 10^{-8}$ Hz is significantly flatter than the short-time-scale ($10^{-2} - 10^{-5}$ Hz) power spectrum derived from EXOSAT observations which in frequency region ($10^{-4} - 10^{-6}$ Hz) has a power index $\alpha = 2.1$ (Hayashida et al. 1998).

The long-term optical variability of the continuum in the UVB band was studied by Lyuty & Doroshenko (1999). They showed that a long photometrical minimum in years 1984–1989 separates two active phases: 1968–1988 (Cycle A) and 1989–2000 (Cycle B). The decrease of brightness continued in 2000 and at the end of 2000 year the brightness of the variable component reached almost the same values as in 1987–1988 (Doroshenko et al. 2001). These phases are also seen in JHKL-bands (Lyutyi, Taranova & Shenavrin 1998).

The PSD of the NGC 4151 optical flux variations in 1968–1987 was studied by Terebizh, Terebizh & Biryukov (1989). It was found that PSD in the frequency range $10^{-4} - 2 \times 10^{-2} \text{ day}^{-1}$ (time interval from 50 days to 30 years) corresponds to flicker noise with slope ≈ 1 in logarithmic scales and the light curve may be interpreted as a result of superposition of flares randomly distributed in time. The behaviour of the structure function (hereafter SF) in the period 1989–1996 was studied by Merkulova, Metik & Pronik (2001), with particular attention paid to the intra-night variability. Collier & Peterson (2001), using the same technique, determined the characteristic timescale as 13_{-5}^{+11} days.

Long timescale trends in optical variability of NGC 4151 were studied by Lyutyj & Oknyanskij (1987) and Fan & Su (1999), on the basis of data covering the period from 1910. Lyutyj & Oknyanskij noted the quasi-periodical changes with typical time 4 and 14 years. Also Fan & Su (1999) claimed the presence of the periodicity, with the period 14.0 ± 0.8 yr, during which both the brightness and the spectral type change. It is not surprising that both groups found the similar quasi-periodical processes in optical light curve because the main data set used by both teams was the same. Some earlier papers also claimed the presence of the periodic variability albeit with other values of the period (e.g. Pacholczyk 1971 - 5.1 years), while other papers argued against any strict periodicity (e.g. Pacholczyk et al. 1983; Terebizh et al. 1989).

The short term multiwavelength variability was best studied by AGN Watch team and summarized by Edelson et al. (1996). They concluded that significant and correlated variability was observed in X-ray, UV and optical band, with phase differences consistent with zero lag and normalized variability amplitude decreasing with increasing wavelength. They calculated the power spectrum in UV on timescales of ≈ 0.2 –5 days and showed that the power spectrum is falling down rapidly at short timescales and the bulk of the variability power is on timescales of days or longer.

In the present paper we reanalyze the optical and X-

ray data available in the literature which cover 90 and 25 years, correspondingly. Such a broad dynamical range allows us to draw conclusions about the character of the flow and the possible nature of the instabilities responsible for the observed variability.

2 OBSERVATIONAL DATA

2.1 Optical band

The observational data in optical region used in the present paper come from different sources.

Long data sets were collected by the team at the Crimean Station of the Sternberg Astronomical Institute (1968–2000), the Special Astrophysical Observatory in the Caucasus (1997–2000), and the Maidanak Observatory of the Ulugbek Astronomical Institute in Uzbekistan (1990–2000). For convenience, in further text we will refer to these data as Crimean data. The data collected in three bands (U, B and V) cover the period from 1968 till 2000. The data points are not distributed uniformly since the source was at some periods unobservable at the sites involved but the sets consist of about 1150 points in each colour thus providing an exceptionally long and well covered light curve for an AGN. The light curve and the discussion of the variability amplitude and colour changes were presented by Lyuty & Doroshenko (1999) and Doroshenko et al. (2001). Additionally, shorter data set (about 300 points during 1989–1999) in the infrared band R is also available (Doroshenko et al. 2001).

Shorter, but more densely spaced data set was taken from the AGN Watch team (Kaspi et al. 1996). This data cover only 98 days but it adds 62 points to the long set. Continuum flux in the spectral band 4560–4640 Å was fitting to the flux in B-band of Crimean data set using regression relation based on 17 common dates of observations.

Most of the oldest data were obtained by Pacholczyk et al. (1983) from the old Harvard & Stewart photographic plates. These data cover the period from 1910 till 1968. Besides those observations we used data from Fitch, Pacholczyk & Weymann (1967), Cannon, Penston & Brett (1971), Penston et al. (1971) & Oknyanskij (1978, 1983). Comparison of the photographic magnitudes between various data sets and with Crimean photoelectric data in B-band for overlapping dates of observations allowed us to reduce the photographic data into photoelectric B-bands magnitudes.

As a result, in the B-band we obtained rather long data set covering 1910–2000 years. We must note that the similar work of gathering all photographic observations was made by Lyuty and Oknyanskij (1987), but in comparison with this work we added more photoelectric observations after 1984. Next compilation of the 1910–1991 data was prepared by Longo et al. (1996) but they used even more of the old data from heterogenic sources and interpolated the data in order to obtain equally spaced data points which lead to large errors so finally they had to ignore the first 30 years of observations. The full combined light curve of the NGC 4151 nucleus in B band is shown in Fig.1.

From this curve it is clearly seen that the variability in 1910–1978 based on photographic data is similar in character to the variability in 1968–1989 covered by photoelectric observations. Therefore, we considered the old data as generally reliable.

The overall character of the variability is not constant over the entire data set - the behaviour of the optical curve in 1990-2000 rather differs from the one in 1910-1985. The evolution up to 1985 can be represented by a single parabolic-type curve with maximum flux about 75-80 mJy and with superimposed on it more fast variations of brightness. In 1935 there was (if the photographic magnitudes were estimated correctly) the strongest flare which lasted only 10-15 days. A less intense flare happened in 1946 but it is based on a single point. The evolution in 1990 - 2000 looks itself like a single giant outburst but this change in variability character happened in the middle of the period covered by the photoelectric data.

All the optical data were used for analysis via computing the structure function (SF) and power spectrum density (PSD).

2.2 X-ray data

The data in 2-10 keV X-ray band also came from different papers and databases which were collected using different satellites. Fluxes were corrected for absorption. The observed time coverage is from October 1974.

The data points during 1975-1992 were taken from Papadakis & McHardy (1995). Out of 133 their data points, most came from Ariel V Sky Survey, and others were taken from literature including observations by EXOSAT, GINGA, OSO-8, HEAO-1, TENMA and Ariel VI satellites. Some additional points (in period May 1987 - May 1995) were found in Yaqoob & Warwick (1991) and Yaqoob et al. (1993) and were also taken from the Tartarus Database of ASCA observations¹. We corrected their fluxes for absorption using the HEASARC's online W3PIMMS Version 3.1 flux converter² as well as papers of Weaver et al. (1994) and Edelson et al. (1996). Data from the first three years of RXTE observations during October 1998 - November 1999 were taken from Markowitz & Edelson (2001). The observational data given in that paper in *counts/s* were transformed into unabsorbed fluxes via the mean luminosity of 300-day window given in the paper. We supplemented those gathered data with three long sequences. Two EXOSAT lightcurves were obtained from Ian M. McHardy for the paper by Czerny & Lehto (1997). These data cover 10 and 11 July 1983 and 15 May 1985, with rate sampling 100 s. Third sequence, from ASCA satellite, covers the period from 12 till 23 May 2000, with the rate sampling 32 s. The measurements in *counts/s* were again converted to fluxes using the mean luminosity for an appropriate data sequence.

All X-ray points used by us for further analysis are showed in Fig.2 with open circles.

3 METHODS

3.1 Power spectrum

We attempt restoration of the underlying power spectrum $|F|^2$ of the active nucleus from its observed light curves, i.e. from the product of the true light curve and the sampling

¹ <http://tartarus.gsfc.nasa.gov/>

² <http://heasarc.gsfc.nasa.gov/>

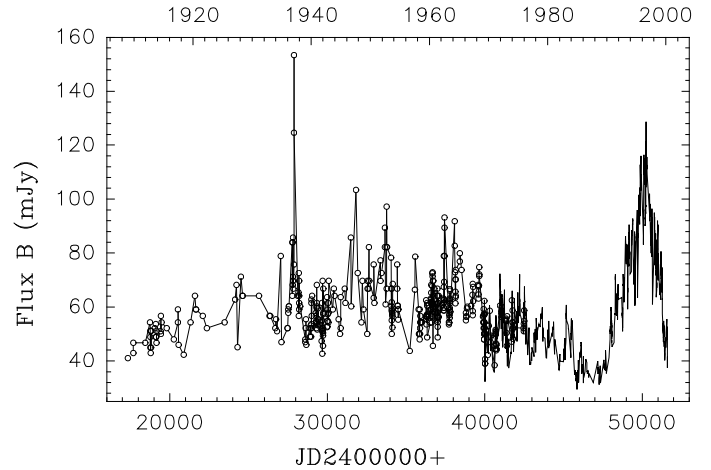


Figure 1. The lightcurve of NGC 4151 in B band from the historical plate data (open circles connected with a continuous line) and Crimean observations (solid line).

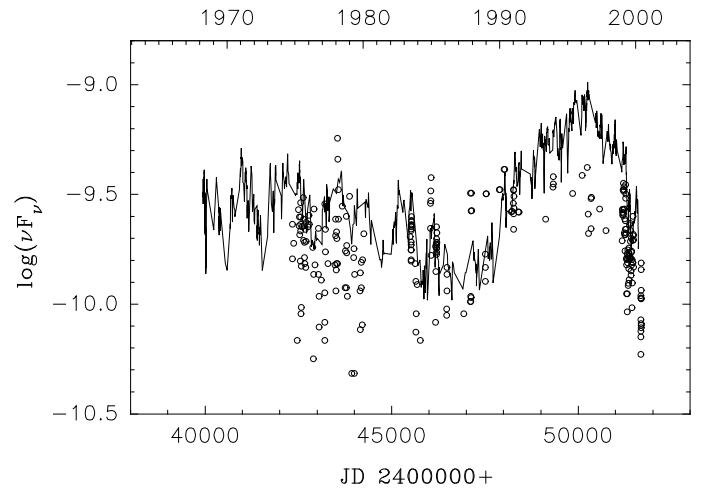


Figure 2. The lightcurve of NGC 4151 (νF_ν) in U band (solid line) and in X-ray band (2-10 keV absorption-corrected flux, open circles).

function. Direct analysis of observations yields the observed power spectrum $|G|^2$, i.e. the underlying spectrum affected by the window function $|W|^2$. These functions obey an exact relation in the Fourier transform space:

$$G = F * W \quad (1)$$

where $*$ denotes the convolution and F , G and W are Fourier transforms of the underlying and observed light curves and of the sampling function. For long and nearly uniformly sampled observations $|W|^2$ approaches the delta function and G approximates well F . For non-uniform sampling the shape of the window function becomes complex, with broad wings and many local maxima. In such case it is difficult to obtain a solution of Eq. (1) for F as it involves deconvolution of the sampling transform W . To cope with such a situation we apply the code CLEAN of Roberts, Lehár & Dreher (1987) which determines the true power spectrum through the cleaning process based on the Fourier transform of the window function.

For uniformity, all data points are converted from magnitudes to flux units, when necessary, and the average value is subtracted. The normalized power spectrum density (hereafter NPSD) is computed according to the description by Hayashida et al. (1998)

$$NPSD(f) = \frac{1}{\langle s \rangle^2} a(f) a^*(f) \times T, \quad (2)$$

with

$$a(f) = \frac{1}{n} \sum_{i=1}^n s_i \exp(2\pi i f t_i), \quad (3)$$

where s_i is the value of the flux at the time t_i , T is the length of the data set and $\langle s \rangle$ is the mean value of the flux. Therefore, the integrated NPSD gives half of the fractional variance.

3.2 Structure function

For analysis of our time series we also used the structure function (SF). The application of SF allows us to study both stationary and nonstationary processes. The SF was introduced by Kolmogorov in 1941 for analysis of the statistical problems connected with turbulence theory (Kolmogorov 1941a,b). In astronomical practice, the wide application of the SF to time-series analysis begun in the middle eighties (e.g. Simonetty, Cordes and Heeschen 1985; Paltani, Courvoisier & Walter 1998; Kataoka et al. 2001).

As a rule, the astronomers use only the first-order structure function (SF_1). By definition the structure function of the first-order is a mean square of difference $[x(t) - x(t + \tau)]$:

$$SF_1(\tau) = M[(x(t) - x(t + \tau))^2], \quad (4)$$

where $x(t)$ is random process and τ is time shift. Since we do not use higher order structure functions, we denote SF_1 as SF , for simplicity.

In the case of a stationary random process the (SF) is identically related with autocorrelation function:

$$SF(\tau) = 2D[x(t)] \times [1 - ACF(\tau)], \quad (5)$$

where $D[x(t)]$ is variance of the process and ACF is the autocorrelation function.

The slope of the SF changes with time interval τ . If the measurement errors are neglected, on the shortest time scale the variability can be well approximated by a linear trend, and then $SF \propto \tau^2$. For long time scale the slope of the SF becomes flatter and in the limit when $\tau \rightarrow \infty$ the structure function saturates: $SF \rightarrow 2D[x(t)]$. The addition of measurement errors to the random process increases SF by the value $2D_{err}$ where D_{err} is the variance of the measurement errors.

Many processes are stochastic in nature. For some processes, like fractional Brownian motion, the SF show a power law dependence on τ . Some processes can be represented as a superposition of a large number of random impulses of deterministic form (shot noise). Sub-group of those processes which are characterized the $PSD(f) \propto 1/f^\gamma$ are called flicker noise. If γ takes values from 1 to 3, then in this case the structure function $SF(\tau) \propto \tau^b$ where b takes values from 0 to 2, following the relation

$$\gamma = b + 1. \quad (6)$$

The structure function analysis was done using program package by S.G. Sergeev from Crimean Astrophysical Observatory. The whole time interval was divided into equal bins in logarithmic scale and for each bin we found such pairs of observations with $t_j > t_i$ that their time difference $\tau_k = t_j - t_i$ fitted into the given bin. Next we calculated the value

$$SF(\tau_k) = \sum_{i,j} \frac{[x(t_j) - x(t_i)]^2}{n_k}, \quad (7)$$

where n_k is the number of pairs in k-th bin.

3.3 Autocorrelation function

Generally, for computing the autocorrelation function (ACF) or the cross-correlation function (CCF), either interpolation or discrete methods are used (see Edelson & Krolik 1988). Interpolation method is based on the linear interpolation of a light curve to obtain its value after the shift by the time interval τ , and discrete method is based on collecting the pairs of points corresponding to given bin of time interval τ . Discrete method allows to calculate the errors for correlation coefficient but interpolation method is more effective. In our computations of ACF we again made use of program package by S.G. Sergeev. His method belongs to the class of interpolation method. For any point from the real data a corresponding shifted point is found by linear interpolation or extrapolation, and extrapolation is made adapting $x(t > t_{max}) = x(t_{max})$ and $x(t < t_{min}) = x(t_{min})$ (for more detailed description, see Sergeev et al. 1999).

4 RESULTS

4.1 Stationarity of the data

Question of whether light curves of AGNs covering several decades of years may be considered realizations of a stationary process is interesting *per se* and because of possible influence onto investigations at shorter time scales (e.g. Leighly 1999, Press & Rybicki 1997).

4.1.1 Optical band

Even the visual inspection of the lightcurves of the galaxy NGC 4151 clearly shows some long timescale trends although they become less prominent with an increase of the data length. It can be best studied in the B band since at that colour the lightcurve at disposal is the longest.

We analyzed the longest trends by rebinning the data in one year bins in order not to be biased by the most recent periods with extremely good data coverage in comparison with the earliest data from the beginning of the previous century. We studied the trends both using magnitudes (effectively logarithmic scale) or using νF_ν fluxes (effectively linear scale).

Mean value of the magnitude in the Crimean observations in B band is 11.83. Apart from two major outbursts, the presence of the linear trend is also seen in the data. Linear fit in magnitude scale gives a shift by -0.35 mag during the entire period of observations (32 years). This is comparable to the value of the dispersion in this period, calculated

for unbinned data (0.33). The result is similar if flux (νF_ν) is used: linear trend gives the net brightening by 1.2×10^{-10} erg s $^{-1}$ cm $^{-2}$, with the dispersion equal 1.4×10^{-10} erg s $^{-1}$ cm $^{-2}$. However, if the entire data set of 90 years of data is analyzed, the linear trend acts in the same direction but is much weaker. Systematic shift is only -0.13 mag, or 3.6×10^{-11} erg s $^{-1}$ cm $^{-2}$, with the dispersion unchanged.

This shows that the data is not strictly stationary even on the timescale of 90 years. However, in the longest data set the linear trend is much weaker than the typical amplitude of the variability (in B band) and the assumption of stationarity is roughly satisfied. It is less so in case of shorter sequences, so the power spectra and the structure function may depend on the choice of the data set. This is particularly well known from the studies of X-ray lightcurves of galactic sources (e.g. Uttley & McHardy 2001, and the references therein; for quasar sample see Manners, Almaini & Lawrence 2001).

4.1.2 X-ray band

X-ray data cover only the period from 1974 till 2000, and the older data (till ~ 1986 seem to show larger scatter so the presence or the absence of the long trends is less apparent (see Fig. 2).

We again rebinned the data in one year bins in order to achieve uniform distribution in long timescales and looked for a linear trend in the resulting lightcurve. The mean 2-10 keV flux was equal 1.98×10^{-10} erg s $^{-1}$ cm $^{-2}$ while the linear trend gave the systematic brightening of the source by 4.12×10^{-12} erg s $^{-1}$ cm $^{-2}$, much lower than the dispersion in the data during this period (6.00×10^{-11} erg s $^{-1}$ cm $^{-2}$). The practically perfect absence of the linear trend in the data is partially accidental - more accurate Ginga/ASCA/RXTE data (1978 - 2000) cover the period which started and ended up at very similar level of the activity of the source. Slightly shorter sequences show trends up to almost an order of magnitude stronger but still smaller than dispersion.

Therefore, the X-ray data seem to be more stationary during the observed period than the optical data during the same epoch. However, a few more years of occasional monitoring are needed to confirm such a statement.

4.2 Power density spectrum

4.2.1 Optical band

We analyze first the Crimean data alone, covering the years from 1968 till 2000, in all three colour bands.

The power spectrum in U band (see Fig. 3) shows two separate parts. The overall variability is dominated by a strong component which flattens off at the longest timescales and falls steeply down at intermediate timescales. At the timescales of months, this component is replaced by a relatively flat tail, possibly represented by a power law with an index around 1.0. The long timescales component is relatively well represented with a function $\text{NPSD}(f) \propto (f^2 + f_o^2)^{-4}$, with the characteristic frequency $\log f_o = -3.70 \pm 0.05$.

The same shape is seen in B band. In V band the high frequency tail is steeper and the division between the two

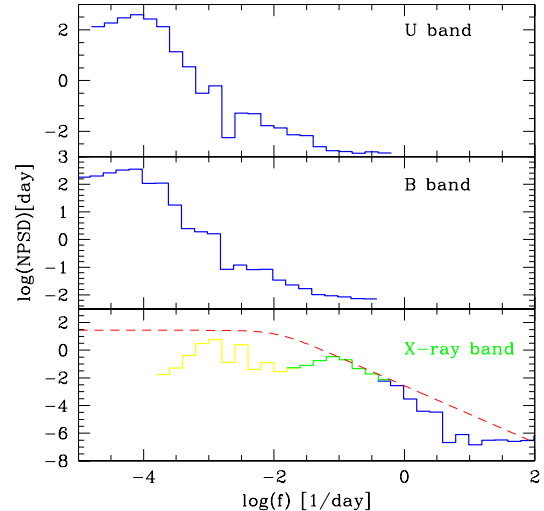


Figure 3. NPSD of NGC 4151: upper panel – U band; middle panel: B band; lower panel: X-ray band; dashed line marks the power spectrum determined by Papadakis & McHardy (1995) and normalized at high frequencies according to results of Hayashida et al. (1998).

components is somewhat less visible, but sudden drop in the power at the timescale of 11 months is still visible.

Since the interesting timescale is rather long, we therefore concentrated on the results derived from the complete set of data in B band, covering the entire 90 years. The result is shown in Fig. 3.

We see again two components: one above ~ 1 year (i.e. $\sim \log f < -2.5$ d $^{-1}$), dominating the total optical power, and one below ~ 1 year. The long timescale component is well represented by a function $\text{NPSD}(f) \propto (f^2 + f_o^2)^{-3}$, with the characteristic frequency $\log f_o = -3.85 \pm 0.05$. This value is very close to the value determined in the U band. The high frequency tail has a slope ~ 1 .

We replotted the resulting NPSD in the form of *Power* \times *Frequency* diagram (see Fig. 4) in order to show better the dominating timescales. We also subtracted the estimated level of the data noise. It shows well the dominating role of the years-timescale component but it also shows the presence of the separate month/days-timescale component. In this plot we see that there may be a high frequency roll-over to the last component at about $\log f = -1$. It would agree with the characteristic timescale determined by Collier & Peterson (2001). The two components are separated by a minimum at about 500 days.

Lyuty & Doroshenko (1999), analyzing the data from the period 1968-2000, argued that there are two cycles of activity in NGC 4151 which differ considerably with respect to the level of variability: first one from 1968 till 1988 (cycle A) and other from 1989 till the present time (cycle B). Since the duration of the outburst B - the dominant feature in the optical lightcurve (see Fig. 1) - coincide with the character-

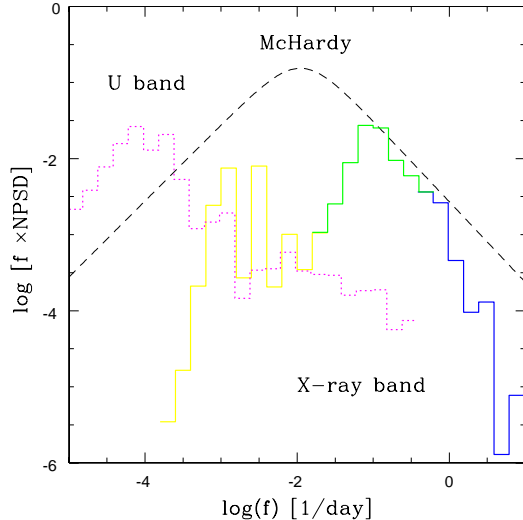


Figure 4. The NPSD multiplied by the frequency showing best where most of the power comes in: dotted line - B band, continuous line - 2-10 keV band. Dashed line marks the power spectrum determined by Papadakis & McHardy (1995) and normalized at high frequencies according to results of Hayashida et al. (1998).

istic frequency seen in our analysis we repeated this analysis for the data set in B band without the cycle B.

The NPSD computed without the cycle B still showed considerable power at $\log f \sim -4$ but relatively more power at $\log f \lesssim -2.8$ so the overall optical NPSD in *Power* \times *Frequency* diagram shows a broader flat hump between -2.8 and -4.2 instead of a relatively narrow peak seen in Fig. 4.

4.2.2 X-ray band

X-ray PSD is distinctively different from the optical NPSD (see Fig. 3). It shows a flattening (or actually even a drop) at much shorter timescales, about 1000 days (i.e. $\log(f) < -2.8$), a relatively flat part between 2.8 and 1.0, and a steeper decrease at $\log(f) > -1.0$. The spectrum might be crudely represented as a broken power law, with slope 1 at intermediate frequencies and rather 2 at higher frequencies. There may be also additional steepening at $\log(f) \geq 0.0$. The normalizations at high frequencies is similar to that obtained by Hayashida et al. (1998). The position of the flattening determined by Papadakis & McHardy (1995) is now in the middle of the intermediate part.

The characteristic features of the shape are again better visible on *Power* \times *Frequency* plot (see Fig. 4). Most of the X-ray power is concentrated between 10 days and 1000 days, with a turnover both at higher and lower frequencies. There may also be a decrease in the variability level at the intermediate timescales of ~ 100 days. Broken power law is not a good representation of the power spectrum but if applied, it gives the low and high frequency turning points as $\log(f)$ equal -2.75 and -0.9, correspondingly. The low fre-

quency characteristic point may not be determined accurately due to the problems discussed in Section 4.1.2.

Optical variability in the 10 - 1000 day timescales has roughly similar character to X-ray variability, although the normalized PSD is considerably lower in the optical band. However, above the timescales of 2000 days the optical variations 'take over', strongly dominating the variability of the source.

4.3 Structure function

The analysis via the structure function was applied to the Crimean data, covering the years from 1968 till to 2000 in UBV bands and to the combined photographic plus photoelectric data in B band covering the years from 1910 till to 2000, to AGN Watch data and also to X-ray data, gathered by us from the literature.

4.3.1 Optical band

Let us consider only Crimean data. Fig. 5 shows SFs for the optical flux in various colour bands drawn by open circles. One can see that SF has almost ideal noise form in V, with the slope $b \approx 0.7$ for time scale of variability from 1 to 4500 days. Such value of b shows that the dominating process is a single shot noise process. But in the U and B bands the shape of the SF is more complex, and a clear break in the SF is seen at about 30 - 50 days, with much steeper slope at short timescales and a flatter one in long timescales. The results of Merkulova et al. (2001) shows that the steep slope continues down to the timescales of minutes. It can again indicate that in these two time intervals two different processes operate. We therefore measured separately the slope in time interval from 1 to 30 days and in time interval from 80 to 4700 days (see Table 1). We see that in V band a single moderate slope of 0.7 provides a good representation of the variability in all timescales shorter than 4500 days (12.3 years) but at shorter wavelengths the two slopes are significantly different. This difference is most visible in U band. We can also note that the structure function of AGN Watch data in the continuum fluxes at $\lambda 4600 \text{ \AA}$ converted to fluxes in B band is in rather good agreement with the SF for B band of Crimean data (open and filled circles respectively in the third panel of Fig. 5). The traces of similar structure are only barely seen in V band.

One of the important characteristics of the structure function is the point which marks the beginning of plateau at the long time lags. This time scale gives the maximum time scale T_{max} of correlated signals or, equivalently, the minimum time scale of uncorrelated behaviour. From Fig. 5 we can see that the SF reaches plateau at $\log \tau \approx 3.2 - 3.6$, i.e. about 1600 - 4500 days.

As it was shown by Lyuty & Doroshenko (1999), there are two cycles of activity in NGC 4151 which differ considerably with respect to the level of variability: first one from 1968 till 1988 (cycle A) and other from 1989 till the present time (cycle B). Therefore we repeat our analysis for those two cycles separately.

All slopes of the SF are presented in Table 1. Spectral bands are marked in column (1), time interval for correlated variability are specified above columns (2 - 4) and above

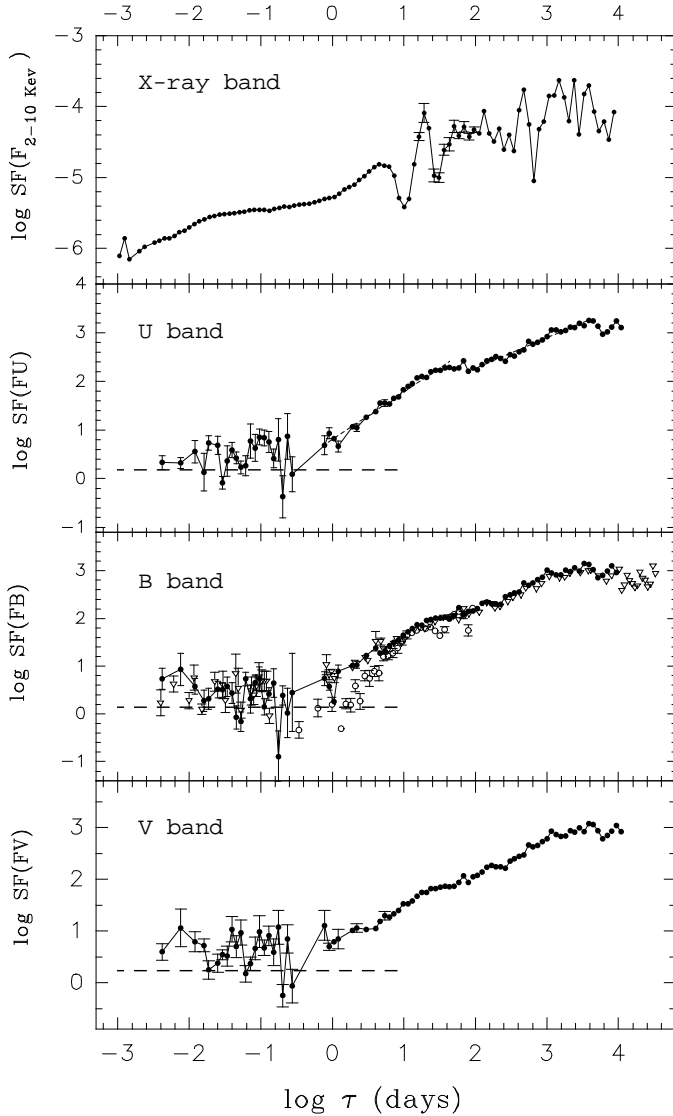


Figure 5. The structure function for NGC 4151: upper panel - X-ray band, second panel - U band, third panel - B band (Crimean data - filled circles; AGN Watch - open circles; photographic data - triangles), lowest panel - V band. Dashed line shows the level of SF due to the measurement error in the data.

columns (5 – 7), slopes b and errors of slope, $\sigma(b)$, are shown in column (2), (3) and (5), (6), and correlation coefficients r for the corresponding regressions are in column (4) and (7).

We see that the properties of the lightcurves (SF slopes) are significantly different in the two cycles. During the cycle B the slope difference between the short and long timescales is rather moderate, although a feature around 50 days is present. The plateau for long time shifts begins at $\log\tau=3.2$ - 3.4. During the cycle A the difference of the slopes is profound in all colour bands, with the long timescale slope being very flat (see Fig. 6), suggestive of weak long timescale trends. This is caused by the fact that in cycle A we do not see a single large outburst but rather a number of weaker eruptions superimposed on a weak longer trend. The localization of T_{max} , which is the time scale when SF reaches plateau, is less clearly seen in the cycle A than in the cycle B, or in the composite data.

In order to resolve the issue what processes are responsible for the variability of source we restore to the longest data sets available in B band. Earlier we have remarked that the historical curve from 1910 till to 1975 is similar to the B-band light curve in 1968-1988. It seems as if cycle A started at 1910, or earlier, and continued up to 1989. Since the photographic data is of relatively low accuracy, and the number of data points is small in comparison with photoelectric measurements performed at the late period of the cycle A, we compute separately the SF only for historical data without mixing them with photoelectric data in that cycle. This structure function corrected for the constant contribution due to measurement error (8.5%) is shown in the third panel of Fig. 5 with open triangles. We see that the slopes of both structure function are similar within the errors. Although the length of historical data set is about 25200 days ($\log\tau = 4.4$), the plateau begins earlier, at about $\log\tau = 3.2$ (corresponding to the time interval 1600 days). So the existence of the plateau is not an artifact of too short data but its presence is supported by long observations.

The flattening observed in SF at 1600-4500 days (4 - 12 years) corresponds well to the flattening observed in the optical PSD. The change of the slope at some point is also clearly seen in both cases, although it does not happen precisely at the same timescales. The fast component sets off below ~ 30 days according to SF studies while it is rather ~ 500 days according to NPSD.

The maximum time scale T_{max} of correlated signals derived from the plateau of the structure function is about 1600-4500 days while it is about 5000 days from the power spectra so this characteristic timescale of the optical variability can be considered as determined rather reliably and can be used in further discussion.

4.3.2 X-ray band

The shape of the SF in the X-ray band can be approximately represented by a single power law with a slope ~ 0.3 (see Fig. 5). A flattening at the timescales above ~ 1000 days is not excluded but not strongly required. Errors in this part of the plot are large. Minor changes of the slope are also seen at $\log\tau$ around -1.8 and 0, and a complex structure is visible at timescales of 10 days.

There is therefore a good correspondence between the SF and the NPSD in this band although the quality of the data seem to be lower than for the optical data which provided better coverage (longer timescale covered more uniformly) for the long timescale variability study. The presence of the two characteristic timescales - 1000 days and 10 days - should be confirmed by subsequent monitoring.

4.4 Autocorrelation function

We supplement the analysis by showing the autocorrelation function for the full data set in U band and in the X-ray band. The difference between the two plots is remarkable. We see from Fig. 7 that X-ray flux shows very good correlation only at extremely short timescales below 10 days. At timescales of order of 10-1000 days, corresponding to a hump in a X-ray NPSD (see Fig. 4), a broad shoulder replaces the sharp peak and falls down slowly. A significant minimum in

Table 1. Structure function slopes b in various colour bands, data sets, and timescales.

Cycle A (25.03.1968 - 03.07.1988)						
Band	(1 - 30)days			(80 - 4700) days		
	b	$\sigma(b)$	r	b	$\sigma(b)$	r
U	1.16	0.07	0.97	0.19	0.04	0.68
B	1.16	0.08	0.95	0.20	0.04	0.69
V	0.85	0.05	0.96	0.18	0.04	0.65
Cycle B (11.02.1989 - 13.03.2000)						
Band	(1 - 30)days			(80 - 1500) days		
	b	$\sigma(b)$	r	b	$\sigma(b)$	r
U	0.96	0.04	0.98	0.73	0.03	0.98
B	0.94	0.04	0.98	0.74	0.04	0.98
V	0.73	0.04	0.98	0.76	0.04	0.98
R_J	0.73	0.09	0.86	0.83	0.06	0.95
Cycles A+B (25.03.1968 - 13.03.2000)						
Band	(1 - 30)days			(80 - 4700) days		
	b	$\sigma(b)$	r	b	$\sigma(b)$	r
U	1.01	0.03	0.99	0.62	0.02	0.99
B	1.00	0.05	0.98	0.63	0.02	0.98
V	0.75	0.03	0.99	0.64	0.03	0.98
Photographic observations + Cycles A+B (5.03.1910 - 13.03.2000)						
Band	(1 - 30)days			(80 - 4700) days		
	b	$\sigma(b)$	r	b	$\sigma(b)$	r
B	0.72	0.04	0.97	0.58	0.03	0.97
X-rays (20.10.1974 - 05.01.2000)						
Band	2 min - 4.5 days			(14 - 4400) days		
	b	$\sigma(b)$	r	b	$\sigma(b)$	r
2-10 keV	0.27	0.01	0.96	0.29	0.07	0.57

b - slope of the SF in considered timescale range, $\sigma(b)$ - error of the slope, r - correlation coefficient from linear regression

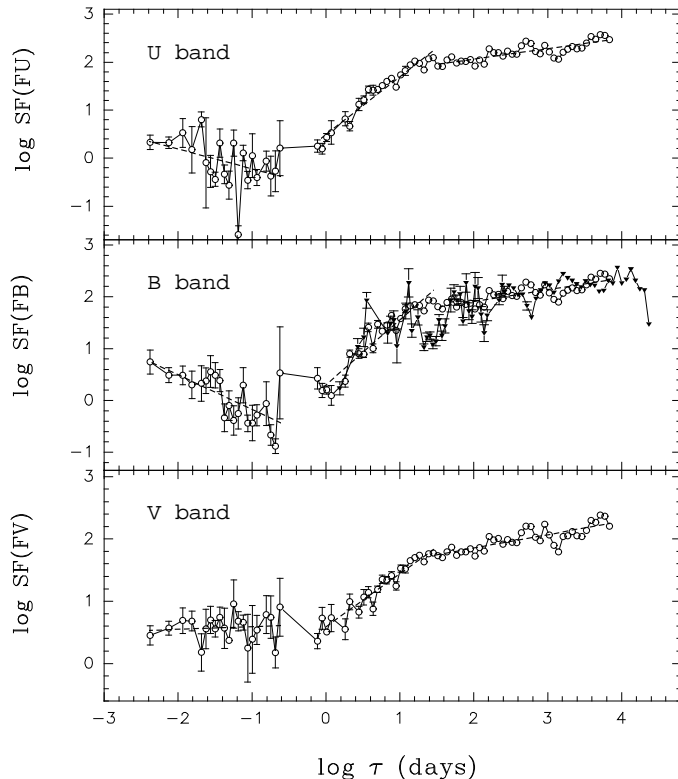


Figure 6. The structure function for the cycle A (Crimean data – open circles, photographic data - filled triangles).

the correlation is seen at a timescale of ~ 215 days, which multiplied by 2 corresponds well to the first minimum in NPSD, zero level is reached ~ 500 days. It is consistent with not completely flat SF at such a long timescales (see Table 1). The correlation reaches zero at 400 days, giving timescales of 800 days, in agreement with the presence of considerable power in NPSD down to timescales of ~ 1000 days.

U band autocorrelation function does not show a similar structure and falls down steadily, crossing 0 at a time lag of 1650 days and indicating the characteristic timescale of about 3300 days. This is again in rough agreement with the determination from SF (1500 - 4500 days) and NPSD (~ 5000 days).

5 DISCUSSION

5.1 Character of optical and X-ray variability

Our results indicate that there are two variability mechanisms operating in the Seyfert galaxy NGC 4151. Optical variations are dominated by the component with the characteristic timescale about 4000 ± 1000 days (11 ± 3 years). In X-ray band the dominant power seems to correspond to timescale range between 10 and 1000 days. Traces of this variability are also seen, but as a separate variability component, in the optical band.

Our results therefore support the early claim of Be-

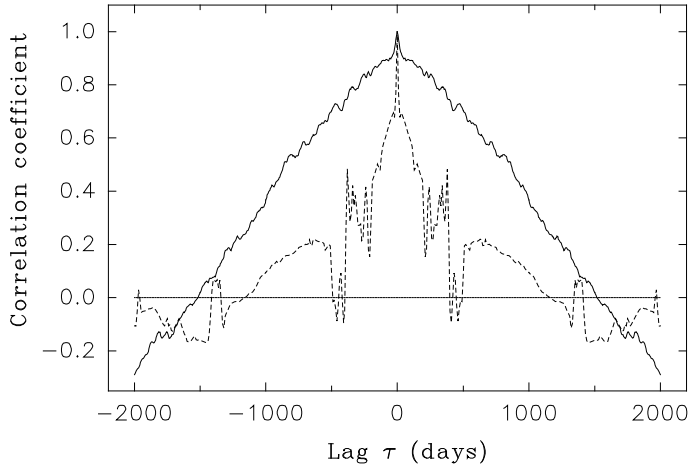


Figure 7. Autocorrelation function in U band (continuous line) and in the X-ray band (dashed line).

lokon, Babadzhantz & Lyutyi (1978) based on much more limited data.

The shortest characteristic timescale seen in our data in both energy bands is in agreement with the timescale 13_{-5}^{+11} days determined by Collier and Peterson (2001). These authors did not find the long timescale component because their data for NGC 4151 covered only 99 days. Their conclusion about the overall similarity between the optical/UV variability and X-ray variability *in short timescales* agrees with our results although our results are not particularly accurate in that range.

The dominant role of the long timescales in the optical band cannot be an artifact of the difficult analysis since it is actually apparent from Fig. 1. The actual value of the characteristic timescale is strongly influenced by the recent outburst (cycle B) lasting from 1978 till 2000 although the traces of similar timescales are present in the older data as well, superimposed on low amplitude longer trend.

The lack of longer than ~ 3 years trends in the X-ray data obtained from NPSD is less secure and the absence of longer timescales is also not apparent from the SF analysis. Large error of the early measurements make this determination rather difficult. A few more years of further monitoring will resolve this issue definitively.

5.2 Correlation of optical and X-ray luminosity

Long data sets provided also an opportunity to better study the correlation between the U band and the 2-10 keV X-ray emission. Our results are shown in Fig. 8. The correlation seems to be surprisingly poor. Short timescale study of UV and X-ray variability of Edelson et al.(1996) showed a very strong coupling during 10 days of monitoring. Noticeable correlation was found by Perotti et al. (1990) between the

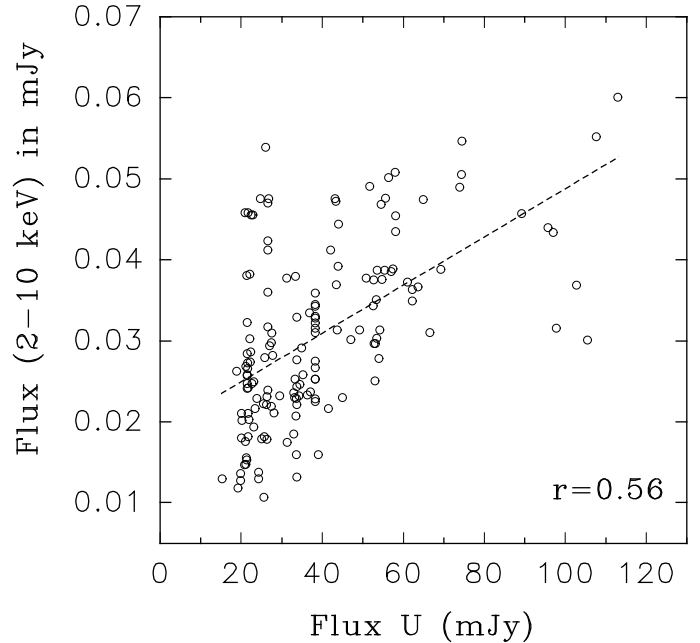


Figure 8. The correlation between the optical flux in U band and the X-ray flux; dashed line marks the linear fit. The value of the correlation coefficient r is rather low.

hard X-ray 35 keV flux and the optical flux. Oknyanskij (1994) discussed the issue of the dependence of broad band correlations on the luminosity state of the nucleus and he found that in the low state in 1983-1986 correlations are more significant than in high state in 1975-78.

Therefore, we also looked for correlation between the X-ray data gathered by us and our U fluxes in different parts of light curve. From our Fig. 2 it is well seen that part of X-ray (2-10 keV) light curve in 1974-1991 does not correlate with optical fluxes in U while the part from Dec.1993 -1999 correlates better. The correlation coefficient is $r = 0.71 \pm 0.06$ ($n=68$). Therefore our conclusion is that the correlation is better when the source is generally brighter, in opposite to Oknyanskij (1994). It most probably suggest that there is a problem with the determination of the X-ray flux in the oldest X-ray data. The source is heavily absorbed, and the absorption varies, so the older instruments with lower spectral resolution and sensitivity could not determine the intrinsic spectrum, and the unabsorbed 2-10 keV flux. This problem should probably not affect our determination of the long timescale trends in X-ray luminosity since the drop of the power below the timescales of ~ 3 years is quite rapid.

5.3 Comparison with NGC 5548

Although the power spectra in the X-ray band are available now for a number of AGN the variability in the optical band

was quantitatively studied only for the Seyfert galaxy NGC 5548. Therefore, we can only compare the results for the two Seyfert galaxies: NGC 4151 and 5548.

We compare the structure functions in U, B, V, R_J bands of NGC 4151 with the results for NGC 5548 obtained by Doroshenko et al. (2001). They use a Crimean data from 1990 to 2000 for U, B, V and from 1991 to 2000 for R_J band.

Our result is that *SF* of NGC 4151 in U and B bands has two slopes *b* independently of the period of observations (see Table 1 and Figures 5, 6, , whereas *SF* of NGC 5548 has a single slope in all bands. The values of the slope, *b*, are: 0.72 ± 0.02 (for U band), 0.69 ± 0.02 (B), roughly similar to our results for the long timescale behaviour in Cycles A+B. The similarity is even more clear if we restrict ourselves to the the Cycle B of NGC 4151 where we also found a single slope in the V band although somewhat steeper (0.75 ± 0.03 in NGC 4151 versus 0.65 ± 0.03 in NGC 5548). The long timescale slope in V band in the whole data set for NGC 4151 was identical to that found in NGC 5548 (0.64 ± 0.03 (V) in NGC 4151 versus 0.65 ± 0.03 in NGC 5548). However, the timescales of *SF* flattening are significantly different in the two objects: in NGC 4151 they are about $\log \tau = 3.6$ [day] while in NGC 5548 they are considerably shorter, just below $\log \tau = 3.0$ [day].

We can also compare the normalized power spectrum density of NGC 4151 in optical band (Fig. 4) with NGC 5548 given by Czerny et al. (1999) (Fig. 7). We can see a maximum in *Power* \times *Frequency* representation in both objects. However, for NGC 4151 it is at $\log \nu \simeq -3.7$ [1/day] while in NGC 5548 it is again at $\log \nu \simeq -3$. Therefore, the longest characteristic timescale is by a factor of 4 - 5 longer in NGC 4151 than in NGC 5548.

The mass difference itself cannot explain in a simple way the difference in the long timescale behaviour of the optical flux. Approximate analysis of the disk radius predominantly contributing to a given spectral wavelength gives

$$r \propto L_{bol}^{1/3} M^{-2/3} \quad (8)$$

(see e.g. Siemiginowska & Czerny 1989) and the thermal timescale related to this radius is

$$\tau \propto L_{bol}^{1/2} M^{-1} \quad (9)$$

so with somewhat larger luminosity and smaller mass of NGC 5548 in comparison to NGC 4151, as taken from Czerny et al. (2001), the formula gives an expected timescale by a factor of 3 shorter for NGC 4151 while the observed one is actually longer.

We also compare the normalized power density spectrum of NGC 4151 in X-ray (2-10 keV) band (Fig. 4) with NGC 5548 given by Chiang et al. (2000). The overall shape of PSD in both objects is similar. PSD increases to the first point of inflection at $\log \nu \simeq -2.3$ for NGC 5548 and $\log \nu \simeq -2.7$ for NGC 5548. Then the shape is approximately flat to the second point of inflexion, where PSD start to decrease. This point has $\log f \simeq -0.9$ for NGC 4151 and $\log f \simeq -0.7$ for NGC 5548, so the total width of the flat *Power* \times *Frequency* part is equal to 1.6 decades for NGC 5548 and 1.8 decades in NGC 4151.

The mass of the central black hole estimated from reverberation studies are equal to $\log M = 7.83$ for NGC 5548 (Peterson & Wandel 1999) and $\log M = 7.08$ for NGC 4151 (Wandel, Peterson & Malkan 1999), while variability studies

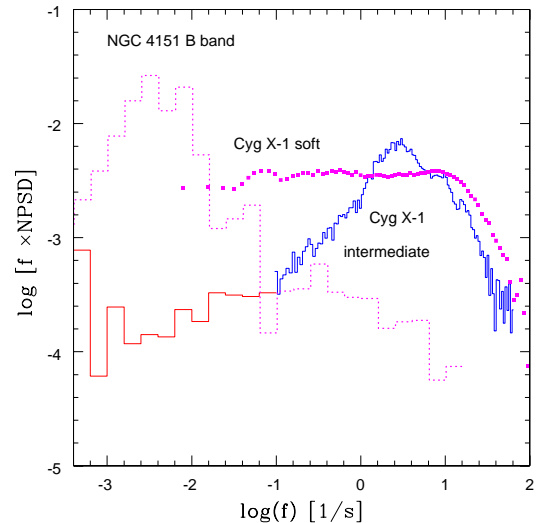


Figure 9. The NPSD for Cyg X-1 in the soft state (filled squares, from Gilfanov et al. 2000) and in the intermediate state (continuous histogram), together with the NPSD for NGC 4151 in the optical band shifted horizontally by 6.3 to account for a mass difference between the two sources (dotted histogram).

of Czerny et al. (2001) gave the values equal 7.39 and 7.57. The difference of 0.2 in the position of the X-ray NPSD between NGC 5548 and NGC 4151 obtained in the present paper again suggests that the black hole in NGC 4151 is rather likely to be more massive (by a factor 1.5) than the black hole in NGC 5548, in opposite to reverberation results.

5.4 Comparison with Cyg X-1

The comparison between the galactic objects and AGN is not simple. Observed spectra generally consist of two principal spectral components: soft bump usually interpreted as the accretion disk emission and a power law interpreted as a result of Comptonization by a hot optically thin plasma. In AGN these components are well separated: the first one dominate optical/UV emission while the second one dominate in X-ray band. In galactic sources both are seen in X-ray band but their dominant role depend on the luminosity state of the source. Therefore, the power spectrum of a GBH in the hard power-law dominated state should be compared with the X-ray power spectrum of an AGN while the power spectrum of a GBH in the soft or intermediate disk-dominated state should be compared with the optical power spectrum of an AGN.

X-ray power spectra of AGN are generally quite similar to power spectra of galactic objects in their hard state (see e.g. Czerny et al. 2001 and the references therein). The power peak in *f* \times *NPSD* diagram is broad, covering about 2 decades, and its position on the frequency axis depends on the mass of the black hole and can well be used for the mass determination (Hayashida et al. 1998; Czerny et al. 2001).

Our determination of the X-ray power spectrum (Fig. 4) is not considerably different from this picture although some substructure might be seen. Therefore, it supports a view that the mechanism responsible for the emission and variability of the power law spectral component are identical for AGN and GBH.

However, a comparison of the optical power spectrum with the power spectra of galactic sources in soft or intermediate luminosity state does not show any striking similarity. In Fig. 9 we show the NPSD in a soft state determined by Gilfanov et al. (2000) and in the intermediate state determined by us using the RXTE data from 30 May 1996 from HEASARC archive (see also Cui et al. 1997). The power is either quite evenly distributed across the broad range of frequencies or a short timescale variability dominates; an analogue of a strong long timescale component dominating the optical power spectrum of NGC 4151 is not seen.

Strong outbursts at timescales from hundreds to a few thousands of seconds are only seen in the microquasar GRS1915+105 (see Belloni et al. 1997). However, this source shows strong jet outflow and therefore it is not a simple analogue of a radio quiet Seyfert galaxy.

5.5 Decomposition of optical lightcurve into fast and slow variability components

The presence of the two separate types of variability - a slow component and a fast component - was already suggested by Belokon, Babadzhanjanz & Lyutyi (1978). Our results from the analysis of the PSD and SF in U and B band based on much better data coverage confirm this result. Therefore, the data is not well represented by sum of a constant component and a rapidly variable component, as suggested by Ulrich (2000). However, those long timescale trends are only seen when appropriately long time sequences are studied.

In order to visualize the presence of the two separate types of variability - a slow component and a fast component - we complement the computations of the optical NPSD and the SF with a simple illustration.

We calculate the smooth long timescale lightcurve at each data point by averaging all available data points separated from a given moment by less than adopted smoothing timescale, ΔT . An exemplary set of such lightcurves for a range of ΔT is shown in Fig. 10. We see that for $\Delta T < 500$ days a number of small outbursts is still seen while for $\Delta T > 500$ days the peak luminosity of the cycle B starts to be smeared.

The value $\Delta T = 500$ days seems to be optimal for the separation of the long and short variability timescale. Adopting this value, we display the short timescale variations by subtracting the smoothed lightcurve from the original one (see Fig. 10, panel (a)). The result is shown in Fig. 10, panel (b). We see that the amplitude of variations display significant trends: it is the smallest around 1988, when NGC 4151 faded, and the highest around 1995, when the source was exceptionally bright. This dependence of the amplitude on the flux was discussed by Doroshenko et al. (2001).

Such trends almost disappear if we plot the normalized lightcurve, i.e. if the value of the flux difference is divided by the value of the flux of the smoothed lightcurve (see Fig. 10, panel (c)). It shows that the variability expressed in per cent is roughly constant, independent on the source

luminosity while the variability amplitude measured in flux units is proportional to the flux at a given epoch. Therefore, this figure provides an illustration of the same fact that was stressed by Uttley & McHardy (2001): normalization of the 'non-normalized' power spectrum computed in short timescales depends on the source luminosity while the NPSD is independent on the luminosity of the source at the analyzed period. This dependence disappears if normalized power spectrum is computed.

We can now compare these trends with variability of Cyg X-1 in disk-dominated spectral state. In Fig. 10 (panel (d)) we show 250 s sequence from the lightcurve of Cyg X-1 in May 30, 1996 (30 yr for NGC 4151 are equivalent to 250 s of Cyg X-1). We see that this lightcurve is definitively different from the original U-band lightcurve (see Fig. 2) but there is some similarity to the lightcurve shown in panel (c) where all the long trends have been removed. Traces of longer trends are still seen, in agreement with the shape of the power spectrum (see Fig. 9), but fast variations dominate. This supports our earlier conclusion that the fast variability may well be connected with the X-ray reprocessing, and the X-ray variability itself is similar in AGN and GBH so the nature of fast variability might be the same in both types of objects.

5.6 Intrinsic variability versus obscuration

A number of authors suggested that the variable obscuration is, at least partially, responsible for the observed variability of AGN (e.g. Collin et al. 1996, Boller et al. 1997, Brandt et al. 1999, Risaliti, Elvis & Nicastro 2001).

This scenario was explored in some detail by Abrassart & Czerny (2000) in a context of short timescale variability caused by random cloud position rearrangement, without any intrinsic change of the luminosity and the covering factor. According to their simple model, such a variability should lead to smaller variations in the optical band than in the X-ray band, consistent with the short timescale behaviour but not with the long timescale trends which show that most power in the timescales of years is in the optical (or possibly UV) band. On the other hand, observed delays between the optical continuum and the emission lines (e.g. Kaspi et al. 1996) and between the optical emission and the infrared emission (e.g. Oknyanskij et al. 1999) show that the variability at the timescales of days is certainly intrinsic to the source, at least partially. The nature of still faster intraday variability seen predominantly in X-rays may be due to obscuration by optically very thick clouds, as in the picture of Abrassart & Czerny (2000). According to this model, the slope of the hard X-ray power law should not change in those timescales but the observational constraints on the change of the slope are weak (the changes of the spectral slope in the timescales of days were detected by Ginga but they may well be attributed to the variable ratio between the intrinsic flux and the constant reflection component - Yaqoob & Warwick 1991, Nandra et al. 1991). Therefore, the intrinsic character of the shortest timescale variability cannot be excluded.

At the longest timescales of years, the variable obscuration is an interesting possibility.

The absorbing column density in Ginga/EXOSAT data seems to be lower when the source is brighter (Yaqoob &

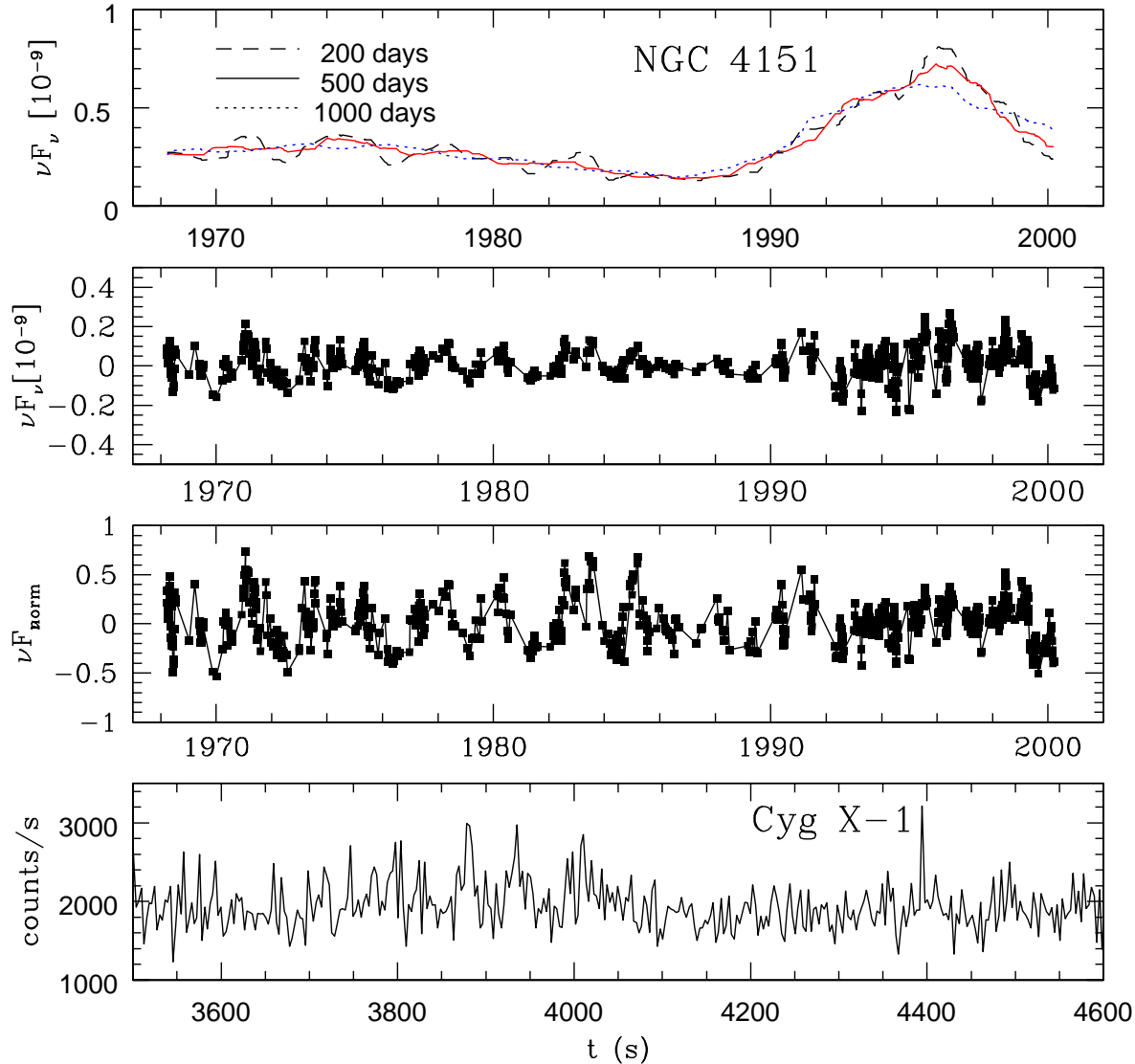


Figure 10. Panel (a): the smoothed lightcurve of NGC 4151 in U band, for the smoothing timescale equal 200, 500 and 1000 days. Panel (b): the lightcurve of NGC 4151 in U band, with the long timescale trend of 500 days subtracted. Panel (c): the normalized lightcurve of NGC 4151 in U band, with the long timescale trend of 500 days subtracted. Panel (d): X-ray lightcurve of Cyg X-1 when the source was in the transition state (May 30, 1996)

Warwick 1991). However, if we look at the most recent and accurate observations no obvious correlation is seen. In December 1993 when the AGN Watch monitoring was done the source was bright in U band (~ 75 mJy; Kaspi et al. 1996, Crimean data) and the intrinsic X-ray column was 3.5×10^{22} cm^{-2} (Edelson et al. 1996). In the beginning of March 2000 the source was dim in U band (~ 21.5 mJy; Crimean data) and the intrinsic X-ray column determined from the Chandra data was 3.7×10^{22} cm^{-2} (Ogle et al. 2000).

IUE monitoring during 18 years, which covered both the very low state around 1988 and the luminosity peak in the middle of B outburst around 1995 showed a factor over 12 increase in the flux although the UV line CIV1550 showed lower amplitude, of a factor of 5 (see Fig. 11 of Ulrich

2000). It might suggest that the continuum variations are additionally enhanced by some variations in the absorbing medium, perhaps due to variable ionization although, on the other hand, we do not see directly the driving continuum of the CIV line. Measurements of the NLR show that the X-ray power law component extends down to soft X-rays and it is not much fainter on average that it was during the AGN Watch campaign but NLR does not see UV part of the Big Blue Bump directly so no long timescale constraints on its shape are available (Alexander et al. 1999).

This shows that although the variable obscuration cannot be totally excluded it cannot be the only factor responsible for the observed variability and most of variations are instead intrinsic to the source.

5.7 Comparison with predictions of radiation pressure instability

The presence or absence of the radiation pressure instability in accretion disks is currently under discussion. Resolving it from the theoretical side is quite complex so an alternative approach, from the observational side, is useful.

The strong variability of AGN in optical, UV and X-ray band is a well known but not well understood phenomenon (see Mushotzky, Done & Pounds 1993, Ulrich, Maraschi & Urry 1997). A rapidly increasing attention, however, is paid recently to this issue since it may offer an insight into the geometry of the mixture of hot and cold material surrounding a black hole from the studies of dynamics of the accretion process. Spectral modeling alone does not seem to solve an important issue whether or not the cold accretion disk extends down to the marginally stable orbit without being disrupted and replaced by a hot flow (e.g. Done 2001) and whether the viscous torque operating in the cold disk due to the magneto-rotational instability is (or is not) well represented by the standard αP prescription, leading to the disk instabilities in thermal/viscous timescale.

The observed properties of the X-ray flux indicate some stochastic process (McHardy & Czerny 1987, Czerny & Lehto 1997), which physically can be interpreted as magnetic flares above the cold disk or shocks developing in the hot accreting material. Optical variations are partially caused by reprocessing (although modeling is not simple; see e.g. Rokaki, Collin-Souffrin & Magnan 1993, Kazanas & Nayakshin 2001, Życki & Różańska 2001, Wang, Wang & Zhou 2001) and partially by another process operating in longer timescale. We therefore test if any of the processes are related to the presence of radiation pressure unstable region.

The cold disk variability can be related to the Keplerian timescale, t_K , thermal timescale, t_{th} or viscous timescale t_{visc} of the accretion flow. The first value is universal, and the other two can be computed for a Shakura-Sunyaev disk model. The hot plasma variations may also be related to t_K and t_{th} , although the lack of theory of the hot phase dynamics makes this parameterization less firm.

We now fix the mass of the black hole at $3.7 \times 10^7 M_\odot$, based on variability studies, (see Czerny et al. 2001), and we take the average luminosity to the Eddington luminosity ratio 0.02 resulting from the black hole mass value and the estimate of the total bolometric luminosity. For those parameters, we obtain the radial dependences of those timescales:

$$t_K = 0.18 m_{3.7} r_{10}^{3/2} \quad [\text{d}], \quad (10)$$

$$t_{th} = 1.8 \alpha_{0.1}^{-1} m_{3.7} r_{10}^{3/2} \quad [\text{d}], \quad (11)$$

$$t_{visc} = 4000 \alpha_{0.1}^{-1} m_{3.7} r_{10}^{7/2} \dot{m}_{0.02}^{-2} \quad [\text{d}], \quad (12)$$

where r is expressed in the units of 10 Schwarzschild radii, m in units of $3.7 \times 10^7 M_\odot$, and α in units of 0.1. The mass of the black hole enters the formulae linearly, and the accretion rate affects only the third quantity. In this computations we adopted $\dot{M}_{Edd} = 1.69 \times 10^{18} \times (M/M_\odot) \text{ g s}^{-1}$, and $L_{Edd} = 1.27 \times 10^{38} \times (M/M_\odot) \text{ erg s}^{-1}$, corresponding to the accretion efficiency 1/12.

The extension of the radiation pressure dominated zone was estimated analytically by Shakura & Sunyaev (1973), which gives, for the adopted values of the accretion flow

parameters in NGC 4151 and $\alpha = 0.1$,

$$\begin{aligned} r_{out} &= 91 R_{Schw}, & t_K &= 5.2[\text{d}], \\ t_{th} &= 52[\text{d}], & t_{visc} &= 2.6 \times 10^4[\text{yr}]. \end{aligned} \quad (13)$$

More accurate description of the disk vertical structure, including the proper treatment of the heavy elements impact on the opacity predict smaller radiation pressure dominated, unstable region. We performed the computations using the code described in Janiuk, Czerny & Siemiginowska (2000) (for more details, see Różańska et al. 1999).

The disk (at this value of the black hole mass and mean accretion rate) is expected to be unstable inside the region $r < 66 R_{Schw}$ so the viscous timescale of the global outburst would be still about 8000 years, and the Keplerian and thermal timescales reduce to 3.1[d] and 31[d], correspondingly.

We can now compare those timescales with the characteristic points present in the NPSD and SF both in the optical and in the X-ray band. The derived timescales are related to the Fourier frequencies: $f = (2\pi t)^{-1}$. The factor 2π is important if we want to compare the predicted timescales with the characteristic frequencies in the shape of the NPSD. Therefore, observed characteristic frequencies (1/10, 1/1000 and 1/4000 d⁻¹) translate into 1.6 d, 160 d, and 640 d, respectively.

The ratio of the first two timescales (100) well agrees with the ratio of the Keplerian or thermal timescales at the outer edge of the radiation pressure dominated region and at the marginally stable orbit. Adopting smaller value of the viscosity (0.02) we can reach the agreement between the observed X-ray NPSD and SF with the range of thermal timescales present in the unstable part of the disk. The requested value of the viscous parameter α is close to the value obtained from spectral fits to the data for NGC 5548 (0.03, Kuraszewicz, Loska & Czerny 1997).

The coincidence of the timescales is interesting but most probably accidental. From the study of GBH we know that X-ray production region is not related to the presence of radiation pressure dominated zone. Cyg X-1 with its accretion rate \dot{m} around 0.02 does not develop any radiation pressure region inside a disk.

The timescale dominating the optical variability is significantly longer than the thermal pulsation timescale in the unstable region (640 days vs. 31 days for $\alpha = 0.1$). Viscous parameter required in order to match these two values is extremely low: 0.005. On the other hand, viscous timescale is much longer than the observed timescale (8000 yr vs. 11 yr!). However, viscous timescale depends very strongly on the radius. Disk evolution would proceed in much shorter timescale if the disk instability does not operate in the entire unstable zone. In computations of Janiuk, Czerny & Siemiginowska (2000) performed for a galactic black hole outbursts always started at the inner edge of the disk and usually never reached the outer part of the unstable zone. Recent computations of the outburst of an accretion disk under the influence of radiation pressure for the following set of parameters: black hole mass $10^8 M_\odot$, accretion rate 0.06 and viscosity parameter α 0.1 gave outbursts lasting about 11 years (Szuszkiewicz 1999). Those computations seems to support a view of frequent outbursts starting at the inner edge of the disk and not propagating beyond the inner $\sim 10 R_{Schw}$. Computations, however, did not cover the full cycle due to

numerical problems so they do not provide yet a fully satisfactory answer.

Summarizing, the lack of strong long timescale (hundreds of seconds) variability and the lack of radiation pressure dominated zone in Cyg X-1, when compared with the presence of long timescale variations and the disk unstable zone in NGC 4151, favours the radiation pressure scenario. Analysis of the optical variability of NGC 5548 supported this view as well (Czerny et al. 1999). On the other hand, clearly the effect of the disk variability on the X-ray emission is weak, and the predicted disk thermal timescales for NGC 4151 are rather too short by an order of magnitude to match the observed timescale dominating the optical band.

Therefore, the observed variability seems to be consistent both with disrupted disk scenario and with a cold disk extending down to the marginally stable orbit, although in the first case the viscosity parameter α in the disk has to be small (0.005) and in the second case the disk outbursts cannot propagate through the entire instability zone.

6 CONCLUSIONS

Our study of the 90 years of the optical data and 27 years of the X-ray data for NGC 4151 using the NPSD and the SF technique, give the following results:

- variability properties in the optical and X-ray band are essentially different
- X-ray variations are predominantly in the frequency range $1/10 - 1/1000 d^{-1}$
- optical variations are dominated by a component with a frequency $1/4000 d^{-1}$ (or 12 years), with the additional short timescale component related to X-ray variability
- long timescale optical variability may be caused by radiation pressure instability in the accretion disk although the observed timescale seems to be an order of magnitude longer than expected
- the presence of long timescale variability in NGC 4151 and the absence of analogous variability (in timescales of hundreds of seconds) in Cyg X-1 favours the radiation pressure mechanism
- the radial extension of the X-ray production region is similar in NGC 4151 and Cyg X-1 so the possible presence of radiation pressure dominated region in NGC 4151 and its absence in Cyg X-1 does not affect the X-ray production

ACKNOWLEDGEMENTS

We thank S.G. Sergeev for his permission to use the program package for data analysis and J. Lehar for making the code CLEAN publicly available. We also acknowledge a help with Cyg X-1 data and many enlightening discussions with Piotr Życki. This work was supported in part by grants 2P03D 016 18 (BCz & ZL) and 2P03D 018 18 (ASC) of the Polish State Committee for Scientific Research (KBN).

REFERENCES

Abrassart A., Czerny B., 2000, *A&A*, 356, 475

- Aleksander T., Strurm E., Lutz D., Sterberg A., Netzer H., Genzel R., 1999, *ApJ*, 512, 204
- Belloni T., Mendez M., King A.R., van der Klis M., van Paradijs J., 1997, *ApJ*, 479, L145
- Belokon E.T., Babadzanjantz M.K., Lyutyi V.M., 1978, *A&ASS*, 31, 383
- Boller, Th., Brandt W.N., Fabian A.C., Fink H.H., 1997, *MNRAS*, 289, 393
- Brandt J.C., et al., 2001, *AJ*, 121, 2999
- Brandt W.N., Boller Th., Fabian A.C., Ruzsolkowski M., 1999, *MNRAS*, 303, L53
- Cannon R.D., Penston M.V., Brett R.A., 1971, *MNRAS*, 152, 79
- Chiang J., et al., 2000, *ApJ*, 528, 292
- Collin-Souffrin S., Czerny B., Dumont A.-M., Życki P.T., 1996, *A&A*, 314, 393
- Collier, S., Peterson, B.M., 2001, *ApJ*, 555, 775.
- Cui W., Zhang, S. N., Focke, W., Swank, J. H., 1997, *ApJ*, 484, 383
- Czerny, B., Lehto, J.H., 1997, *MNRAS*, 285, 365
- Czerny, B., Nikolajuk, M., Piasecki, M., Kuraszkiwicz, J., 2001, *MNRAS*, 325, 865
- Czerny B., Schwarzenberg-Czerny, A., Loska, Z., 1999, *MNRAS*, 303, 148
- Doroshenko, V.T., et al. 2001, *AstL*, 27, 65
- Done C., 2001, *Adv. Space Res.* (in press, astro-ph/0012380)
- Edelson R. et al. 1996, *ApJ*, 470, 364
- Edelson R., Krolik, J.H., 1988, *ApJ*, 333, 646
- Evans, I. N., Tsvetanov, Z., Kriss, G. A., Ford, H. C., Caganoff, S., Koratkar, A. P., 1993, *ApJ*, 417, 82
- Fan, J.-H., Su, C.-Y., 1999, *ChA&A*, 23, 22
- Fitch W.S., Pacholczyk A.G., Weymann R.J., 1967, *ApJ*, 150, 67
- Gilfanov M., Churazov E., Revnivtsev M., 2000, *MNRAS*, 316, 923
- Hayashida K., Miyamoto, S., Kitamoto, S., Negoro, H., Inoue, H., 1998, *ApJ*, 500, 642
- Janiuk, A., Czerny, B., Siemiginowska, A., 2000, *ApJ*, 542, L33
- Johnson, W.N., McNaron-Brown, K., Kurfess, J. D., Zdziarski, A. A., Magdziarz, P., Gehrels, N., 1997, *ApJ*, 482, 173
- Kaspi S., et al. , 1996, *ApJ*, 470, 336
- Kataoka J., et al., 2001, *ApJ*, (in press); astro-ph/0105022
- Kazanas D., Nayakshin S., 2001, *ApJ*, 550, 655
- Kolmogorov, 1941a, *Dokl.Acad.Nauk.SSSR*, v.30,p.229
- Kolmogorov, 1941b, *Dokl.Acad.Nauk.SSSR*, v.32, p.19
- Kriss, G.A., Davidsen, A.F., Blair, W.P., Bowers, C.W. Dixon, W.V. et al. 1992, *ApJ*, 392, 485
- Kuraszkiwicz J., Loska Z., Czerny B., 1997, *Acta Astr.*, 47, 263
- Leighly, K., 1999, *ApJSS*, 125, 297
- Longo G., Vio R., Paura P., Provenzale A., Rifato A., 1996, *A&A*, 312, 424
- Lyuty, V.M., Doroshenko, V.T., 1999, *Astron. Lett.*, 25, 341
- Lyutyj, V.M., Oknyanskiy, V.L., Chuvaev, K.K. 1984, *Sov.Astron. Lett.*, 10, 335
- Lyutyj, V.M., Oknyanskiy, V.L. 1987 *Astron.Zhurnal*, 64, 465
- Lyutyi, V.M., Taranova, O.G., Shenavrin, V.I. 1998 *Astron. Lett.*, 24, 199
- Manners J., Almaini O., Lawrence A., 2001, *MNRAS* (in press; astro-ph/0110461)
- Markowitz, A., Edelson, R., 2001, *ApJ*, 547, 684
- McHardy I.M., Czerny B., 1987, *Nat.*, 325, 696
- Merkulova N.I., Metik L.P., Pronik I.I., 2001, *A&A*, 374, 770
- Mushotzky R.F., Done C., Pounds K.A., 1993, *ARA&A*, 31, 717
- Nandra K., et al., 1991, *MNRAS*, 248, 760
- Ogle et al. 2000, *ApJ*, 545, L81
- Oknyanskiy V.L., 1978, *Perem. Zvezdy*, 21, 71
- Oknyanskiy V.L., 1983, *Astron.Circuliar*, 1300, 1
- Oknyanskiy V.L., 1994, *Astrophysics and Space Science*, 222, 157
- Oknyanskiy V.L., Lyuty V.M., Taranova O.G., Shenavrin V.I., 1999, *Astronomy Letters*, 25, 483

- Pacholczyk, A.G., 1971, ApJ, 163, 449
 Pacholczyk, A.G., et al., 1983, Astroph. Letters, 1983, 23, 225
 Paltani, S., Courvoisier, T.J.-P., Walter R., 1998, A&A, 340, 47
 Papadakis I., McHardy, I.M., 1995, MNRAS, 273, 923
 Penston M.V., Pérez, E. 1984, MNRAS, 211, 84
 Penston M.V., Penston, M. J., Neugebauer G., Tritton K. P., Becklin, E. E., Visvanathan, N., 1971, MNRAS, 153, 29
 Perez et al. 1998, ApJ, 500, 685
 Perotti F. et al., 1990, ApJ, 356, 467
 Peterson B.M., Wandel A., 1999, ApJ, 521, L95
 Press, W. H., Rybicki, G. B. 1997, in Astronomical Time Series, ed. D. Maoz, A. Sternberg, & E. M. Leibowitz Dordrecht, Kluwer, p. 61
 Pronik S. G., Sergeev V.I., Sergeeva E. A., 2001, ApJ, 554, 245
 Reina, C., Tarengi, M., 1973, A&A, 26, 257
 Risaliti G., Elvis M., Nicastro F., 2001, ApJ (submitted)
 Roberts, D.H., Lehar J., Drehner J.W., 1987, AJ, 93, 968
 Rokaki E., Collin-Souffrin S., Magnan C., 1993, A&A, 272, 8
 Różańska A., Czerny B., Życki P.T., Pojmański G., 1999, MNRAS, 305, 481
 Sergeev, S.G., Pronik, V.I., Sergeeva, E.A., Malkov, Yu.F., 1999, ApJSS, 121, 159
 Shakura N.I., Sunyaev R.A., 1973, A&A, 24, 337
 Siemiginowska A., Czerny B., 1989, MNRAS, 239, 289
 Simonetty J.H., Cordes J.M., Heeschen D.S., 1985, ApJ 1985, 296, 46
 Szuszkiewicz, E., 1999, Mem.S.A.It, 70, 95
 Terebizh V.Yu., Terebizh A.V. & Biryukov V.V., 1989, Astrofizika, 31, 75
 Wandel A., Peterson B.M., Malkan M.A., 1999, ApJ, 526, 579
 Wang, J.-X., Wang, T.-G., Zhou, Y.-Y., 2001, ApJ, 549, 891
 Ward, M.J., Geballe, T., Smith, M., Wade, R., Williams, P., 1987, ApJ, 316, 138
 Weaver, K.A., Yaqoob, T., Holt, S.S., Mushotzky, R.F., Matsumoto, M., Yamauchi, M., 1994, ApJ, 436, L27
 Wu, Ch.-Ch., Weedman, D.W. 1978, ApJ, 223, 798
 Yaqoob, T., et al, 1993, MNRAS, 262, 435
 Yaqoob, T., Warwick, R.S., 1991, MNRAS, 248, 773
 Ulrich, M.-H., 2000, A&ARv, 10, 135
 Ulrich, M.-H., Maraschi L., Urry M.C., 1997, ARA&A, 35, 445
 Uttley, P., McHardy, I.M., 2001, astro-ph/0103367
 Zdziarski, A.A., Johnson, W.N., Magdziarz, P., 1996, MNRAS, 283, 193
 Życki P.T., Różańska A., 2001, MNRAS, 325, 197

This paper has been processed by the authors using the Blackwell Scientific Publications L^AT_EX style file.